ACS OMEGA

http://pubs.acs.org/journal/acsodf

Mini-Review

Colloidal Quantum Dots in Very-Long-Wave Infrared Detection: Progress, Challenges, and Opportunities

Yilu Qin, Tianle Guo,* Jingjing Liu,* Tie Lin, Jianlu Wang,* and Junhao Chu

Cite This: *ACS Omega* 2023, 8, 19137−19144

Read Online

ACCESS | Metrics & More | Article Recommendations

ABSTRACT: The very long wave infrared (VLWIR) is an electromagnetic wave with a wavelength range of 15−30 μm, which plays an important role in missile defense and weather monitoring. This paper briefly introduces the development of intraband absorption of colloidal quantum dots (CQDs) and investigates the possibility of using CQDs to produce VLWIR detectors. We calculated the detectivity of CQDs for VLWIR. The results show that the detectivity is affected by parameters such as quantum dot size, temperature, electron relaxation time, and distance between quantum dots. The theoretical derivation results, combined with the current development status, show that the detection of VLWIR by CQDs is still in the theoretical stage.

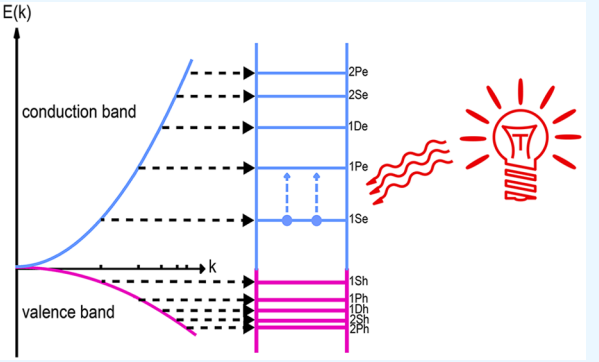

INTRODUCTION

Infrared cameras can see objects in a dark environment in a passive manner (seeing without being seen) through targets' own blackbody radiation. It has been applied in various fields such as infrared guidance, infrared monitoring, autonomous driving, night driving, mine rescue, medical imaging, etc. In all infrared wavelengths, the very-long-wave infrared (VLWIR) range attracts more and more attention due to growing interests in space exploration and commercials. Specifically, in the field of deep space exploration, in the future, VLWIR could also be used for spectral analysis of exoplanets to determine their composition. According to Planck's radiation law, low-temperature objects are more difficult to detect because of the lower radiation emittance and longer maximum radiation wavelength of low-temperature objects. This makes VLWIR photodetectors very important in deep space detection and target tracking outside the atmosphere, because dust features such as carbon-rich asymptotic giant branch (AGB) stars, post-AGB objects, and planetary nebulae (PNe) located in the Milky Way fall within the VLWIR range.[1] For atmospheric monitoring, VLWIR is rich in information about humidity and CO_2 level and provides information about cloud structure and temperature distribution in the atmosphere. This information can be used to analyze the entrance parameters of other spectral bands, so it is also very important.[2] In the soil containing silicon dioxide, the resttrahlen effect will display a high reflectivity spectral band in the very long wave range, so the very long wave can also be used in soil detection.[3]

Nowadays, the predominant VLWIR detectors in spaceborne scientific research are BIB (blocked-impurity-band) detectors,[4] while detection of theater ballistic missiles (TBM) during their midcourse phase is mainly through extrinsic doping MCT (mercury−cadmium−telluride) detectors.[4] The difficulties in material synthesis, doping control, a low operating temperature (<40 K), and a large-scale flip-bonding process[4] limit the use of VLWIR detectors other than in ultra-high-end applications, such as in the Hubble Space Telescope, James Webb Space Telescope, STSS, etc. Currently, IR detectors are at least 3-fold more expensive than silicon pixel arrays,[4] and VLWIR detectors cost quite a bit more than typical IR detectors. The high cost and hard technology barriers limited a wide scale application. As a result, many researchers are engaged in the pursuit of an alternative VLWIR detector that is possible to mass-produce at a low cost.

The hunt started in the 1970s,[5] by replacing II−VI materials with III−V materials; people believed that the maturity of III−V materials' synthesis would bring mass-produced, high homogeneity bulk materials. It was achieved in quantum well infrared photodetectors (QWIPs).[5] However, because of their one-dimensional quantum confinement, normal incidence is strictly forbidden by the selection rules. Therefore, not only is their quantum yield limited at around 10% but also a complex designed grating[5] is introduced in the fabrication procedures

Received: January 19, 2023
Accepted: April 19, 2023
Published: May 26, 2023

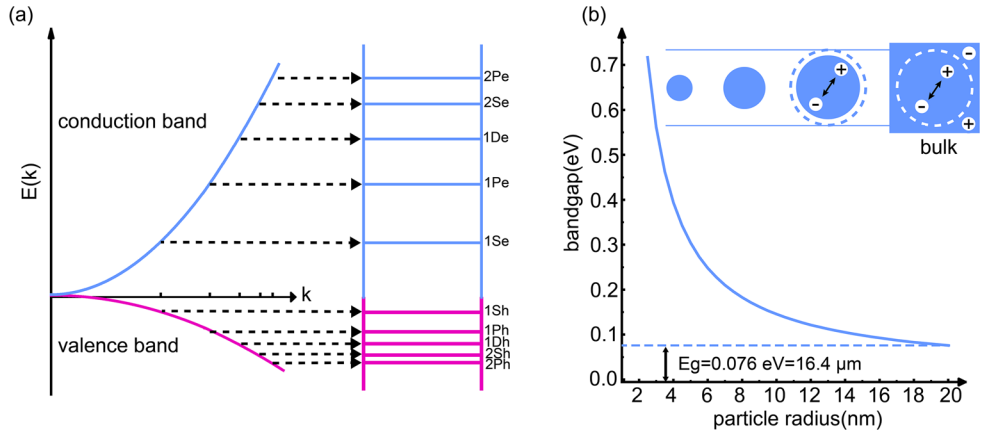

Figure 1. (a) Quantum dots energy levels are discrete and (b) HgTe CQDs band gap.

which counters the purpose of being low cost and mass-produced. Since the 1990s, quantum dot infrared photodetectors (QDIPs) have been considered as a solution to overcoming the forbidden incidence problem.[5] Their quantum confinement comes from all three directions in space. Therefore, the selection rules are completely different, and there is no forbidden incidence anymore in QDIPs. However, there are still shortcomings. The density of Stransky−Krastanov grown QDs (SK-QDs) is far from close-packed, thus the absorption is weak and the cost is as high as that of traditional bulk materials.[5,6] In past decades, colloidal quantum dots (CQDs) have made significant progress in IR detection. As an alternative synthesis method to SK-QDs, CQDs have quite a few advantages, such as a tunable band gap,[7] flexible material and substrate selection,[7] low manufacturing cost,[5,7] and high packing density[7] as well as having the ability to monolithically grow on silicon electronic devices etc. In the past few years, with the help of CQD coating, silicon-based FPA has been realized in the ranges of short-wave infrared (SWIR) and medium wave infrared (MWIR).[8] It is even commercialized with wafer-scale production at SWIR.[8] Nowadays, more and more researchers are engaged in this field and try to push the detection limit to LWIR and even VLWIR. Therefore, with the ongoing fast development of CQDs, long-sought low-cost and mass-produced VLWIR detectors seem within reach.

There have been several reviews on CQD IR detectors recently, but little discussed is the very-long wave infrared range and none describe general sensitivity limits of CQD detectors in the VLWIR range. After introducing CQD detectors and VLWIR light, we briefly review the development of CQDs in VLWIR. We point out that the key for VLWIR is the doping level of materials and then carefully derive the relationship of doping concentration and general sensitivity of CQD VLWIR detectors. In the end, we calculate the influence of sensitivity limits using a few key materials' parameters and evaluate the existing and potential performances of HgTe CQDs for very-long-wave infrared photodetection.

CQDS VLWIR DETECTION AND DEVELOPMENT

Quantum dots are nanometer-size materials with quantum confinement from all three dimensions in space. As a result, electrons and holes would exhibit a discrete (quantized) density of states. When the size of the quantum dots gets smaller, the confinement will be stronger, and the effective bandgap will be increased as well. As is shown in Figure 1a, when applied to infrared detection, such a confinement effect is utilized to open up narrow bandgaps[7,9,10] or even negative bandgaps[9,10] in bulk semiconductors or semimetals.[11] For example, HgTe quantum dots are enabled to detect infrared light by mimicking the iconic HgCdTe (replacing the bandgap tunability from Cd alloying into quantum confinement). Here, for spherical particles with radius R, the effective bandgap shift from the bulk material bandgap is approximately proportional to $1/R^2$. However, as is shown in Figure 1b, when the particle size exceeds the exciton Bohr radius, the quantum confinement quickly disappears. Therefore, through direct bandgap transition, quantum dots in the current stage could not detect anything longer than 16 μm.

To further extend the detection wavelength, one of the ideas is to utilize intraband transitions. Instead of the transition from 1Sh to 1Se, one can easily move to the transition from 1Se to 1Pe. This kind of transition happens when the Fermi level is higher than the lowest electronic state of the conduction band. The 1Se state starts to be occupied by electrons, and then electrons in the 1Se state can move to a higher sublevel, the 1Pe state. The intraband transition was observed in quantum dots decades ago. And in the field of colloidal quantum dots, it was first achieved by Victor Klimov and Duncan McBranch back in 1998. Through ultrafast pump−probe transient absorption experiments, they successfully measured the dynamics of the transition from lowest (1S) electronic state to he first excited (1P) electronic state in CdSe nanocrystals. In 1999, Philippe Guyot-Sionnest et al. observed the intraband transition via infrared pump−probe spectroscopy.[5,12] Later in 2001, the same team also observed the electrically pumped intraband transition[5,13] and found a phonon bottleneck phenomenon through dynamic studies of intraband relaxation.

In order to achieve an intraband transition in quantum dots, a common method is to increase the carrier concentration by doping.[5] In 2008, Norris et al. reviewed the doping synthesis method,[14] theoretically explained the mechanism of doping controls, and pointed out possible pathways to dope quantum dots. In 2012, Sahu et al. improved the cation exchange method by using trioctylphosphine,[15] making it possible to precisely control the amount of doping, which solidified the foundation for the appearance of steady-state intraband transitions in CQDs. In 2014, Deng et al. observed stable intraband transition luminescence in air on HgS CQDs and HgSe CQDs and used intraband for light detection for the first time.[5,7] In 2018,[9,16] Lhuillier and co-workers had shown that, through self-doping, the intraband transition of HgTe quantum dots finally pushed the absorption edge into the VLWIR and even THz range. And

https://doi.org/10.1021/acsomega.3c00403
ACS Omega 2023, 8, 19137−19144

by using As_2S_3 as a ligand, the mobility had reached a milestone of 100 $cm^2 \cdot V^{-1} \cdot s^{-1}$.[9] In 2019, Lhuillier et al. used a mixture of HgSe and HgTe nanocrystals to enhance the transmission characteristics, reduce the dark current, reduce the response time, increase the thermal activation energy, and increase specific detectivity of the intraband CQD photodetector to 1.5×10^9 Jones.[9,17] In 2020, Guyot-Sionnest experimentally showed that the influence of size distribution on intraband photodetectors is greater than that on interband photodetectors.[10] In 2021, Bin Hafiz et al. studied vertically stacked Ag_2Se CQDs and improved the detection rate of the photodetector based on this by 70 times compared with the original Ag_2Se CQDs detector at room temperature.[9] In recent years, the specific detectivities of some kinds of CQDs have been summarized, as shown in Figure 2.[6,11,17−20] It can be seen that they are still far from the

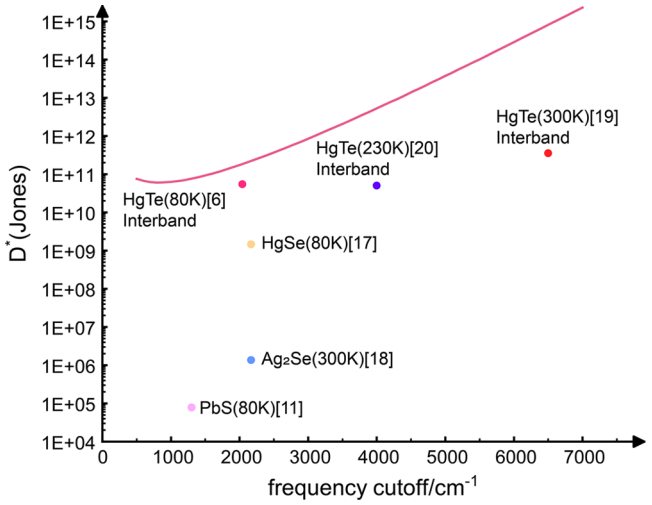

Figure 2. Specific detectivity of BLIP at room temperature and some experimental data.[6,11,17−20]

background limited infrared photoconductor (BLIP) detectivity. To date, even though the research of VLWIR detection in CQDs is still in its early stage and the first prototype VLWIR FPA might still take years to come, a better understanding of intraband transition at longer wavelengths has already been established. CQDs may therefore become one promising candidate in commercialized VLWIR detectors.

DOPING LEVEL AND DETECTIVITY

When quantum dots are doped, the carrier concentration would be substantially increased, and an enhanced dark current is inevitable. But the good news is that a higher dark current does not necessarily lead to a lower detectivity, since the signal is also enlarged. Therefore, it is necessary to know if there exists a specific doping level at which detectivity may reach a maximum. In a simple photoconductive device model, we evaluate the detectivity by the ratio between conductance variance (δG) after IR illumination and average conductance ($\overline{G}$).[11]

Here, we only consider the transition from the confined ground state 1Se state to the first excited state 1Pe state, which most VLWIR detection utilized. To simplify the model, we need to make some assumptions. First of all, the properties of CQD films are the most important, so only the conductance between CQDs is considered, and the ligands and other effects are ignored. Second, the transport between CQDs should be weakly coupled to ensure that the conductance transport between each intraband is independent when there is no transition.[11] Third, after the conductance tends to balance under the illumination, the influence of the transition on the conductance between each independent intraband is also ignored. Fourth, the conductance between two CQDs is the same, and the sum of the conductance should be the linear superposition of conductance between CQDs. As is shown in Figure 3, the conductance of materials is

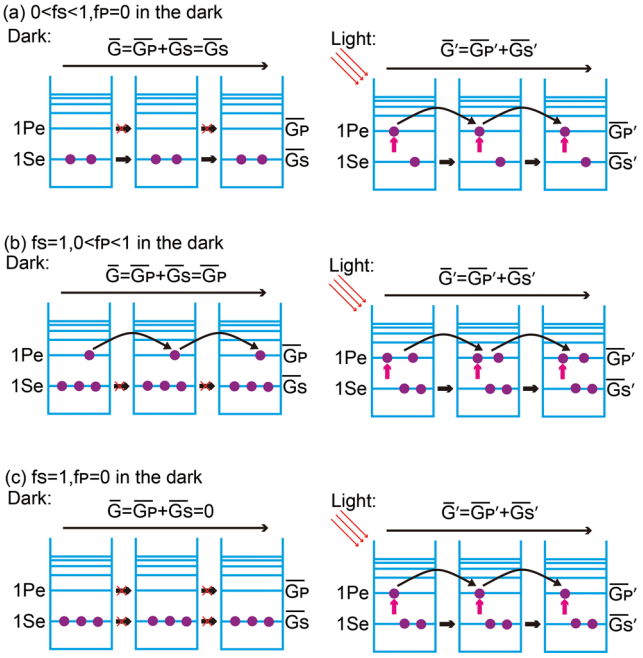

Figure 3. Schematic diagram of conductivity model. (a) The 1Se state is partially occupied in the dark. (b) The 1Se state is completely occupied, and the 1Pe state is partially occupied in the dark. (c) The 1Se state is completely occupied, and the 1Pe state is not occupied in the dark.

G. $\overline{G}$ is the average value of conductance without light exposure, and δG is the change in conductance after exposure to light. In the dark, there are no photogenerated carriers, so $\overline{G}$ is proportional to the dark current. δG is the change in conductance after illumination, which comes from the intraband transition. Therefore, if there is an equal amount of photogenerated charge carriers, the material with a smaller average conductance $\overline{G}$ would have a higher detectivity. Similarly, with the same $\overline{G}$, the larger the δG, the higher the intraband detectivity, so the detection rate can be represented semi-quantitatively by $\delta G/\overline{G}$.

According to Konstantatos et al.'s work,[11] we have the linear expression for conductance:

$$G = \frac{2q_e^{\ 2}}{h} \int A(E)\left(-\frac{\partial f}{\partial E}\right) \mathrm{d}E \tag{1}$$

where q_e is the number of electron charges, and $A(E)$ is the number of propagation modes. $f(E)$ is the Fermi−Dirac distribution and is given by

$$f(E) = \frac{1}{e^{E-E_F/k_BT} + 1} \tag{2}$$

where E_F is the Fermi level, k_B is the Boltzmann constant, and T is the thermodynamic temperature. Then, we immediately get

https://doi.org/10.1021/acsomega.3c00403
ACS Omega 2023, 8, 19137−19144

$$-\frac{\partial f}{\partial E} = \frac{1}{k_B T} f(1-f) \tag{3}$$

For the integral of G, although it looks like a full-space integral, it can be seen that the value of $f(E)$ will converge rapidly when the gap between E and E_F becomes larger. There are two cases to be considered. These two cases are distinguished by whether the 1Pe state is occupied. In the first case, the 1Se state is occupied in the dark, which is the premise of the intraband transition, and the 1Pe state is empty. In the second case, with the rise of the Fermi level, the 1Pe state is occupied in the dark, and the 1Se state is completely occupied in this case. This classifies the transition from the 1Se state to the 1Pe state.

In the first case, the doping level is well-controlled, so that only the 1Se state is occupied. In this case, the 1Pe state is empty without light exposure. An approximation can be made:

$$\overline{G} = \overline{G_S} + \overline{G_P} = \overline{G_S} \ (E_P \gg E_F) \tag{4}$$

and

$$A(E) = A_s \delta(E - E_S) \tag{5}$$

where $\overline{G}_S$ and $\overline{G}_P$ are the average conductance of 1Se and 1Pe states, respectively, without light exposure, E_S is the energy of the 1Se energy level, E_P is the energy of the first excited state 1Pe, and A_S is the total number of modes of the 1Se energy level. We also get

$$\overline{G} = \overline{G_S} = K_S[f_S(1-f_S)] \tag{6}$$

where $K_S = \frac{2e^2}{\hbar} A_S \frac{1}{k_B T}$ and $f_S = f(E_S)$. Assuming that the occupancy probability of electrons after illumination is δf,

$$\overline{G_{S'}} = \overline{G_S} - \delta f \overline{G_S}' \tag{7}$$

where $\overline{G}_{S'}$ is the conductivity due to 1Se electrons under illumination and $\overline{G}_S'$ is the derivative of $\overline{G}_S$ with respect to f_S. Assuming that the photon flux of the excitation light is F and F is small, we then have

$$\delta f = \alpha F f_S \tag{8}$$

where α is the scaling factor. The change value of probability δf can also be regarded as the change value of quantity. Hence, the formula:

$$\overline{G_S}' = K_S(1 - 2f_S) \tag{9}$$

Therefore,

$$\overline{G_{S'}} = \overline{G_S} - \alpha F f_S K_S (1 - 2f_S) \tag{10}$$

and

$$\overline{G_{P'}} = K_{P'}[f_{P'}(1 - f_{P'})] \tag{11}$$

where $\overline{G}_{P'}$ is the conductivity due to 1Pe electrons after illumination,$K_{P'} = \frac{2e^2}{\hbar} A_{P'} \frac{1}{k_B T}$, $A_{P'}$ is the total number of modes of the 1Pe energy level under illumination, and $f_{P'} = \Phi \delta f = \Phi \alpha F f_S$, which is the occupancy probability of the 1Pe state after illumination. Φ is the ratio of the 1Se state degeneracy to the 1Pe state degeneracy. Since F is a small quantity, we get

$$\overline{G_{P'}} = K_{P'} \Phi \alpha F f_S \tag{12}$$

Thus, the conductance after illumination is

$$\overline{G'} = \overline{G_S} + \alpha F f_S (K_{P'} \Phi + 2 f_S K_S - K_S) = \overline{G} + \delta G \tag{13}$$

Therefore, we get

$$\frac{\delta G}{\overline{G}} = \frac{\alpha F f_S (K_{P'} \Phi + 2 f_S K_S - K_S)}{K_S[f_S(1 - f_S)]} = \frac{a f_S + b}{1 - f_S} \tag{14}$$

where a and b are constants.

It can be seen that, when the 1Se state is completely filled, $\delta G/\overline{G}$, reaches a maximum value, which represents the highest detectivity. When $f_S = 1$, the ratio diverges; because this model does not consider other noise sources, only the dark current brought by doping is considered as noise. However, the dark current caused by doping is the largest source of noise, so this model can be regarded as the limit of no other noise sources.

Next, let us consider the second case of doping electrons in the vicinity of the 1Pe state. In an ideal situation, when electrons start to occupy the 1Pe state, the 1Se states should have been fully filled. In this case, we have

$$\overline{G_S} = K_S[f_S(1 - f_S)](f_S \to 1) \tag{15}$$

and

$$\overline{G_P} = K_P[f_P(1 - f_P)] \tag{16}$$

where K_P is for the 1Pe state and has a similar definition to K_S. Under IR illumination, we will have

$$\overline{G_{S'}} = G_S(f_S - \delta f) = \overline{G_S} - \alpha F f_S K_S (1 - 2f_S) \tag{17}$$

and

$$\overline{G_{P'}} = G_P(f_P + \Phi \delta f) = \overline{G_P} + \Phi \alpha F f_S K_P (1 - 2f_P) \tag{18}$$

Therefore, we get

$$\frac{\delta G}{\overline{G}} = \frac{a f_P + b}{f_P(1 - f_P)} \tag{19}$$

where f_P is the electron occupancy probability of the 1Pe state. It can be seen that when $f_P = 0$ or 1, the ratio diverges, and the detectivity is the largest at this time. When $f_P = 1$, absorption will be prevented for the 1Pe state. This implies a physical significance only if $f_P = 0$. So, we reached the same conclusion earlier, that detectivity would reach a maximum when no electron occupies the 1Pe state.

SPECIFIC DETECTIVITY D*

From the discussion above, we now know that when the 1Se state is completely occupied by electrons, while the 1Pe state is completely unoccupied, the dark current stays at a minimum level, and a maximum detectivity can be obtained. In the photoconductive detection model, the Fermi level must be higher than the 1Se state to enable the intraband transition. And unless at absolute zero temperature, electrons in the 1Pe state cannot be fully depleted, which will lead to an increase in dark current. It is assumed that dark current noise occurs when electrons are captured (recombined) and emitted (generated) when a dark current passes through a quantum dot in a certain direction. Dark current noise is essentially generation-complex noise, so the general expression for generation-recombination noise should be satisfied:[6,10,21]

$$i_{n,\mathrm{dark}}^2 = 4 q_e g I_{\mathrm{dark}} \Delta f \tag{20}$$

where q_e is the electron charge, g is the gain, I_{dark} is the dark current magnitude, and Δf is the bandwidth. The dark current can be expressed by the current definition as

https://doi.org/10.1021/acsomega.3c00403
ACS Omega 2023, 8, 19137−19144

$$I_{dark} = J_{dark}A = qnvA \tag{21}$$

where n is the electron concentration, v is the drift velocity of the electron, and A is the cross-section through which the current of the conducting channel passes. The electron concentration can be calculated directly using the density of states and the Fermi–Dirac distribution:

$$\begin{aligned} n &= \int_{E_{Pe}}^{\infty} g_e(E) f(E)\, dE \\ &= \int_{E_P}^{\infty} \frac{1}{2\pi^2}\left(\frac{2m_e^*}{\hbar^2}\right)^{3/2} (E - E_P)^{1/2} f(E)\, dE \end{aligned} \tag{22}$$

where $g_e(E)$ is the density of states, m_e* is the effective mass of the electron, and E_{Pe} is the energy level of the 1Pe state. Since the Fermi level is near the 1Se state, the occupation probability of the 1Pe state is very small, and an infinitesimal approximation can be used. We have

$$f(E) = e^{-E-E_F/k_BT} \tag{23}$$

We immediately get

$$n = 2\left(\frac{k_BTm_e^*}{2\pi\hbar^2}\right)^{3/2} e^{-E_{Pe}-E_F/k_BT} \tag{24}$$

When the distance is set between quantum dots as LP and the transit time as τ_{trans},

$$v = \frac{L_P}{\tau_{trans}} \tag{25}$$

So, the dark current can be expressed as

$$I_{dark} = 2q_e\left(\frac{k_BTm_e^*}{2\pi\hbar^2}\right)^{3/2} \frac{L_P}{\tau_{trans}} e^{-E_{Pe}-E_F/k_BT} \tag{26}$$

It can be seen from the dark current formula that, to reduce the dark current and increase the detection rate, it is necessary to increase the energy level difference between the 1Pe state and the Fermi level, that is, to reduce the electron occupancy probability of the 1Pe state, which is consistent with the conductance model. At the same time, the dark current can also be reduced by lowering the temperature, which is also consistent with this fact.

Then, calculate the gain factor g in the formula.[9] It is assumed that when the dark current noise is generated, the electron density of each state is unchanged, and the probability of an electron being captured is p_c when passing through quantum dots. Then, the modified dark current at the capture emission should be

$$I'_{dark} = (1 - p_c)I_{dark} \tag{27}$$

where I_{dark}' is the size of the dark current where the electrons are captured, and I_{dark} is the dark current when the electrons are not captured. So, the captured current is

$$i_c^{(1)} = p_c I_{dark} \tag{28}$$

Considering that there are $N^{(k)}$ quantum dots in the k direction, we can get

$$I_{dark} = \frac{i_c^{(k)}}{N^{(k)}p_c} \tag{29}$$

Therefore, the gain is

$$g = \frac{1}{N^{(k)}}\frac{\tau_c + \tau_{trans}}{\tau_{trans}} \approx \frac{\tau_c}{N^{(k)}\tau_{trans}} \tag{30}$$

Among them, τ_c is the time of trapping into the potential well, and τ_{trans} is the time of propagation between the two quantum dots. The dark current can be expressed as

$$I_{dark} = 2gq_eN^{(k)}\left(\frac{k_BTm_e^*}{2\pi\hbar^2}\right)^{3/2} \frac{L_P}{\tau_c} e^{-E_{Pe}-E_F/k_BT} \tag{31}$$

The responsivity of the infrared detector can be expressed as

$$R = g\eta\frac{q_e\lambda}{hc} \tag{32}$$

Taking the photosensitive area equal to the cross section through which the current of the conductive channel passes, the specific detectivity can also be calculated:

$$D^* = \frac{R\sqrt{A\Delta f}}{i_n} = \frac{R\sqrt{A\Delta f}}{\sqrt{i_{n,dark}^2}} = \frac{\eta\lambda}{2hc\sqrt{N^{(k)}n}}\sqrt{\frac{\tau_c}{L_P}} \tag{33}$$

It is obvious that specific detectivity is heavily influenced by the energy difference between 1Pe energy and the Fermi level. The larger the difference is, the more electrons have a chance to occupy the 1Se state, leading to a higher dark noise and lower specific detectivity. In the case of our previous assumption, to detect a certain wavelength infrared light, the position of the 1Se state and 1Pe state must be known already. Taking HgTe CQDs as an example, the position of the 1Se state and 1Pe state can be calculated using a simple two-band $k{\cdot}p$ model:[22]

$$E_{Xe} = \frac{1}{2}\left(\frac{\hbar^2k^2}{2m_0} - E_g\right) + \sqrt{\frac{\hbar^2k^2}{2m_0}E_P + \frac{E_g^2}{4}} \tag{34}$$

where k is the wave vector. For the 1Se state, $k = \pi/R$; for the 1Pe state, $k = 4.49/R$, where R is the quantum dot radius. m_0 is the free electron mass/ E_g is the band gap of the material, and E_P is the Kane parameter. Taking $E_g = -0.2$ eV and $E_P = 18$ eV,[22] then we have the energy level difference between the 1Pe and 1Se states. Here, with a simple two-band $k{\cdot}p$ model, we could have drawn a conclusion that, by utilizing intraband transition, we could determine how large the particle needs to be to detect VLWIR. As illustrated in Figure 4, the curve given by the theory is consistent with the trend of some reported experimental data.[23]

Let us continue to calculate the specific detectivity. Now, the only unknown term is the Fermi level. Ideally, the Fermi level should also be determined as well. From what we discussed in last section, the Fermi level should be located between the 1Se and 1Pe states. Therefore, it would be possible to have a fully occupied 1Se state and a completely empty 1Pe state. However, when materials are not at absolute zero temperature, the distribution of electrons would not be ideal, thus it is necessary to know where the Fermi level should be. Here, we use the Nernst equation in electrochemical experiments to estimate the Fermi level:

$$E_F = E^0 + \frac{R_gT}{n_0F}\ln\left(\frac{[Ox]^a}{[Red]^b}\right) \tag{35}$$

where E^0 is the standard electrode potential, R_g is the gas constant, n_0 is the electron transfer number in the electrode

https://doi.org/10.1021/acsomega.3c00403
ACS Omega 2023, 8, 19137−19144

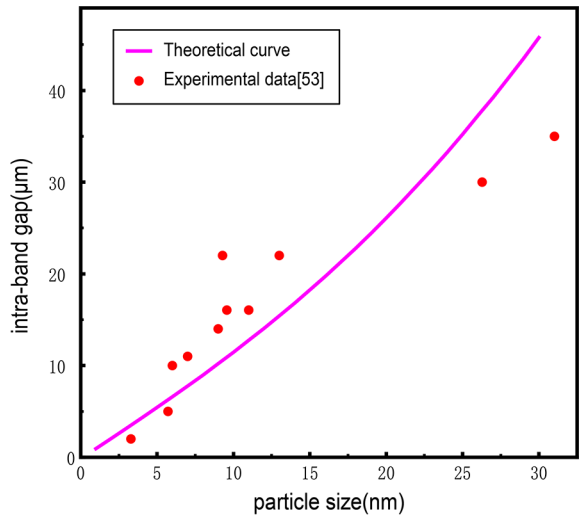

Figure 4. Relationship between intraband gap and particle size of quantum dots. Red dots are some experimental data.[23]

reaction, and F is the Faraday constant. In our hypothesis, since the confined ground state 1Se state is considered to be fully occupied by electrons, it must be satisfied: $E_F - E_{Se} \geq 5k_BT$. At this time, the probability of occupancy is greater than 99.3%. It can be approximated that the 1Se state is completely occupied. Therefore, we now have

$$D^* = \frac{\eta\lambda}{2hc\sqrt{2N^{(k)}\left(\frac{k_BTm_e^*}{2\pi\hbar^2}\right)^{3/2}}}\sqrt{\frac{\tau_c}{L_P}} \frac{}{e^{\frac{\hbar^2(k_{Pe}^2-k_{Se}^2)}{2m_0}+\sqrt{\frac{\hbar^2k_{Pe}^2}{2m_0}E_P+\frac{E_g^2}{4}}-\sqrt{\frac{\hbar^2k_{Se}^2}{2m_0}E_P+\frac{E_g^2}{4}}-5k_BT/2k_BT}} \quad (36)$$

Now, if we assume a perfect condition that external quantum efficiency is 100%, in our target wavelength detection (10 μm, 15 μm, and 20 μm), we have our CQD intraband detection limits at different working temperatures, as is shown in Figure 5a. Using formula 34, we can calculate the size of CQDs through the absorption wavelength. We can also estimate the value of $N^{(k)}$ by assuming the number of CQDs. Therefore, we can roughly estimate the specific detectivity. From the dependence of the specific detectivity on temperature, it can be seen that with only consideration of the dark current from the heat influence, which is a prerequisite for the assumptions of our model, the ideal detectivity at room temperature is only about 10^8 Jones; the performance quickly increases when the working temperature is lower than 50 K. These rough results are quite similar to QWIPs, which utilize the same mechanism: the intraband transition from quantum confinement in a highly doped material. Thus, close proximity to the conclusion of the QWIPs is not surprising. The advantage of CQDs is that the chemical synthesis is simple and CQDs is not limited by the transition selection rule of QWs, which means normal incidence can be probed directly by CQDs.

In addition to the temperature influence, we also estimate the influence from quantum dots' size distribution, which is an important material parameter. The inhomogeneity of CQDs will significantly affect the size of the dark current and thus the detectivity. As is shown in Figure 5b, under a typical Gaussian distribution, it can be clearly seen that with the increase of inhomogeneity, the dark current increases exponentially.

PERSPECTIVE FOR INTRABAND VLWIR CQDS

Nowadays, CQD has proved itself as a promising material for SWIR and MWIR: the commercial SWIR camera was already in the market by SWIR Vision Systems, and MWIR FPA has been reported recently as well.[24] The mass production capability of CQDs detectors with the possibility of a high working temperature could potentially reduce IR sensors' cost to the underlying silicon ROIC while providing many new opportunities for commercial applications. However, in the LWIR and VLWIR range, the application of CQD sensors is hindered by high noise/dark currents. First of all, to achieve VLWIR detection, intraband transition is essential which requires controllably doping impurities to minimize dark current contribution. And it is very difficult to maintain a precise high doping level in CQD systems. Second, unlike traditional quantum well detectors which also utilized intraband transition, most studied CQDs (such as HgTe, HgSe, PbSe, etc.) are a narrow-gap semiconductor; therefore, a noticeable noise contribution due to interband transition will further lower the specific detectivity. In our simple estimation, the best performance of intraband VLWIR (20 um) CQDs reaches 10^{16} Jones at 50 K, which is slightly lower than mainstream VLWIR FPAs such as BIB and MCT detectors. At present, the detectivity of infrared detectors based on CQDs is relatively low in VLWIR,

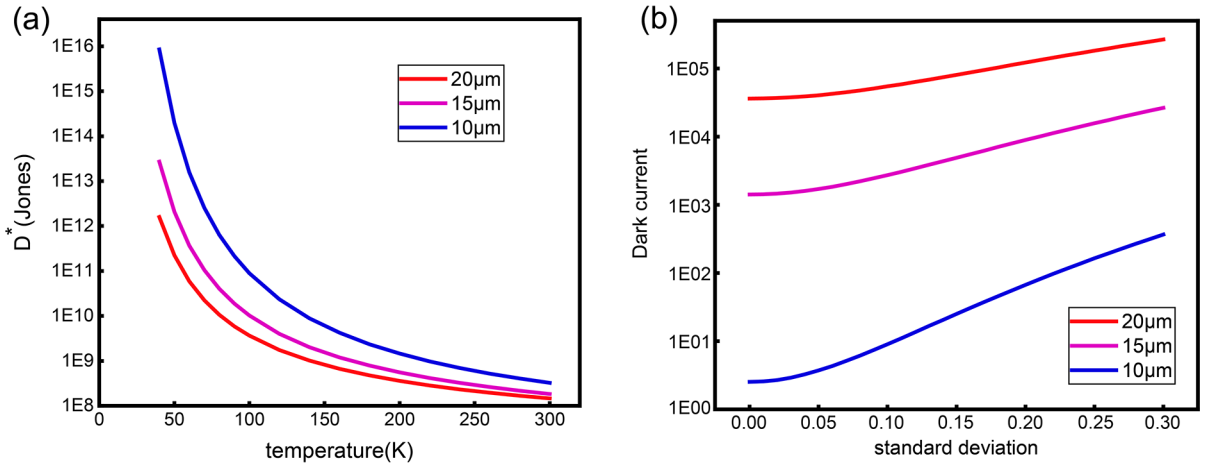

Figure 5. (a) Relationship between specific detectivity and temperature at 10 μm, 15 μm, and 20 μm. (b) Relationship between the dark current and temperature under Gaussian distribution.

https://doi.org/10.1021/acsomega.3c00403
ACS Omega 2023, 8, 19137−19144

which is not competitive in the market; however, it could be improved from several directions.

- Better passivation. Currently, remote doping, using oxidizing and reducing agents, and control of the surface dipole orientation is an alternative doping method in CQD synthesis. However, due to the large surface to volume ratio, any unpassivated site on the surface would alter the doping concentration of CQDs, which greatly increases the dark current of the device. As a result, a fully passivated surface is critical.

- Better size distribution. As is shown in Figure 5, a 10% size distribution might cause a nearly 100% increase in dark current while a 3% size distribution only adds a few percent. Since state-of-the-art colloidal synthesis has provided <3% size distribution for PbS CQDs,[25] one may expect similar progress for any intraband transition CQDs, such as HgTe, HgSe, PbSe, etc.

- Formula 36 shows that the relaxation time is an important parameter that affects the detectability. The long relaxation time is also the advantage of CQDs over quantum wells. Increasing the relaxation time by changing the thickness, temperature, and excitation pulse intensity of CQDs, especially using chemical modification of the nanocrystal surface to alter the electron−hole coupling, can increase the relaxation time and thus the detectivity.

- The distance between two quantum dots can also change the detectivity. The size of the quantum dot determines the wavelength of intraband absorption and cannot be changed. The distance between two quantum dots can only be reduced by producing denser CQDs. By changing the growth parameters and applying surface ligand chemical modification to produce CQDs with smaller distances between quantum dots, the effect of increasing the detectivity of CQD infrared detectors is also achieved in order to meet the applications' requirements.

SUMMARY

This mini-review described the advantages and disadvantages of CQDs in the VLWIR detectors and briefly reviewed the development of intraband transition of CQD photodetection. In the past few years, a decent amount of effort has been put forth to pursue the intraband transition in CQDs as an alternative way to achieve longer wavelength detection. Here, we analyzed the intraband transition from the 1Se state to the 1Pe state, and extended a conductance model in a semiquantitative way to prove the effect of doping on intraband absorption. On this basis, several expressions about dark current and specific detectivity are derived. With the help of the conclusion of the two-band $k{\cdot}p$ model, we also obtained the relationship between intraband transition wavelength and particle size of HgTe CQDs and evaluated the dark current and best specific detectivity of LWIR and VLWIR with varied temperature and size distributions. The results show that, when the particle size is relatively uniform (<5%), the theoretical specific detectivity at 20 um can reach 10^{16} Jones at 50 K but only 10^{8} Jones at room temperature. In addition, the variation of doping concentration and nonuniformity of quantum dot particle size will cause the dark current to increase exponentially. And as a result, a better controlled synthesis is essential.

AUTHOR INFORMATION

Corresponding Authors

Tianle Guo − *State Key Laboratory of Infrared Physics, Shanghai Institute of Technical Physics, Chinese Academy of Sciences, Shanghai 200083, China;* orcid.org/0009-0002-9944-2564; Email: guotianle@mail.sitp.ac.cn

Jingjing Liu − *State Key Laboratory of Infrared Physics, Shanghai Institute of Technical Physics, Chinese Academy of Sciences, Shanghai 200083, China*; Email: liujingjing@mail.sitp.ac.cn

Jianlu Wang − *State Key Laboratory of Infrared Physics, Shanghai Institute of Technical Physics, Chinese Academy of Sciences, Shanghai 200083, China; Frontier Institute of Chip and System, Institute of Optoelectronics, Shanghai Frontier Base of Intelligent Optoelectronics and Perception, Fudan University, Shanghai 200438, China; Hangzhou Institute for Advanced Study, University of Chinese Academy of Sciences, Chinese Academy of Sciences, Hangzhou 330106, China;* orcid.org/0000-0002-5029-8728; Email: jlwang@mail.sitp.ac.cn

Authors

Yilu Qin − *School of Physical Science and Technology, Shanghai Tech University, Shanghai 201210, China; State Key Laboratory of Infrared Physics, Shanghai Institute of Technical Physics, Chinese Academy of Sciences, Shanghai 200083, China*

Tie Lin − *State Key Laboratory of Infrared Physics, Shanghai Institute of Technical Physics, Chinese Academy of Sciences, Shanghai 200083, China*

Junhao Chu − *School of Physical Science and Technology, Shanghai Tech University, Shanghai 201210, China; State Key Laboratory of Infrared Physics, Shanghai Institute of Technical Physics, Chinese Academy of Sciences, Shanghai 200083, China*

Complete contact information is available at: https://pubs.acs.org/10.1021/acsomega.3c00403

Notes

The authors declare no competing financial interest.

Biographies

Yilu Qin received a B.S. degree in physics from Nankai University, Tianjin, China, in 2021. He is currently working toward an M.S. degree in physics with the School of Physical Science and Technology, ShanghaiTech University, Shanghai, China. His research interests include infrared physics, colloidal quantum dots, and topological insulator.

Tianle Guo is currently a postdoc at the Shanghai Insititute of Technical Physics, Chinese Acadamy of Sciences. He received his Ph.D. in physics from the University of Texas at Dallas, U.S.A. in 2019. His research focuses on the electrical transport of infrared colloidal quantum dots and the application of quantum dots in focal plane array cameras.

Jingjing Liu received her Ph.D. in chemistry from Fudan University in Shanghai, China in 2019. She joined the Shanghai Insititute of Technical Physics, Chinese Academy of Sciences as a postdoc in 2020.

Lin Tie is a researcher at the Shanghai Institute of Technical Physics, Chinese Academy of Sciences, focusing on fundamental research and applications of infrared optoelectronic materials and devices. His research interests include low-dimensional semiconductor electronic transport and optoelectronic properties, as well as new mechanisms for optoelectronic response in ferroelectric/2D material composite

https://doi.org/10.1021/acsomega.3c00403
ACS Omega 2023, 8, 19137−19144

structures. He has led or participated in several national and regional research projects and contributed to the development of noncryogenic infrared detection components for the FY3-04 satellite calibration system.

Wang Jianlu is a professor, Cheung Kong Scholar, and doctoral supervisor at the Institute of Advanced Chips and Systems at Fudan University. He received his Ph.D. in microelectronics and solid state electronics from the Shanghai Institute of Technical Physics, Chinese Academy of Sciences in 2010. From 2010 to 2021, he worked as an assistant researcher, associate researcher, and researcher at the Shanghai Institute of Technical Physics, Chinese Academy of Sciences. His main research interests include new optoelectronic materials and detectors, ferroelectric material physics and devices, and optoelectronic sensing chips and systems.

Junhao Chu obtained his bachelor's degree from Shanghai Normal University (SHNU) in China in 1966. Later, he earned his master's and Ph.D. degrees from the Shanghai Institute of Technical Physics, Chinese Academy of Sciences (CAS) in 1981 and 1984, respectively. Between 1986 and 1988, he worked as a Humboldt Fellow at the Technical University of Munich (TUM), Germany. From 1993 to 2003, he served as the Director of the National Laboratory for Infrared Physics. Currently, he is a professor at East China Normal University (ECNU) and the Shanghai Institute of Technical Physics of the CAS. Additionally, he is a member of the CAS. His research interests are centered around semiconductor physics and device technology.

■ ACKNOWLEDGMENTS

This work is Sponsored by the National Key Research and Development program of China (grant no. 2021YFA1200700 (J.W.)), National Natural Science Foundation of China (grant nos. 62105348 (T.G.), 62104235 (J.L.), 62075228 (X.M.)), Shanghai Pujiang Program (21PJ1414900), Strategic Priority Research Program of Chinese Academy of Sciences (grant no. XDB44000000 (J.W.)), and Science Technology Commission of Shanghai Municipality (grant no. 2151103500 (J.W.)). J.L was partially supported by Shanghai Super Postdoctoral Incentive Program.

■ REFERENCES

(1) Gładkowski, M.; Szczerba, R.; Sloan, G. C.; Lagadec, E.; Volk, K. 30-micron sources in galaxies with different metallicities. *A&A* **2019**, *626*, A92.
(2) Gravrand, O.; Mollard, L.; Largeron, C.; Baier, N.; Deborniol, E.; Chorier, P. Chorier, Ph. Study of LWIR and VLWIR Focal Plane Array Developments: Comparison Between p-on-n and Different n-on-p Technologies on LPE HgCdTe. *J. Electron. Mater.* **2009**, *38* (8), 1733−1740.
(3) Ewing, K. J.; Major, K. J.; Sanghera, J.; Kala, R. V.; Howington, S. E.; Ballard, J. Behavior of the Reststrahlen Band in the 17−25 μm Spectral Region in the Diffuse Reflection Spectra of Mixtures of Sand and Silt. *Appl. Spectrosc.* **2020**, *74* (3), 334−339.
(4) Chen, Y.; Wang, B.; Zang, Y.; Zhang, C.; Zhang, H.; Yuan, Y.; Zhou, D.; Hou, L.; Pan, M.; Wang, X. The high-performance imaging verification of Si:P blocked impurity band detector for very-long-wave-infrared spectral range. *IEEE J. Quantum Electron.* **2020**, *56*, 4000506.
(5) Jagtap, A.; Livache, C.; Martinez, B.; Qu, J.; Chu, A.; Gréboval, C.; Goubet, N.; Lhuillier, E. Emergence of intra-band transitions in colloidal nanocrystals. *Opt. Mater. Express* **2018**, *8* (5), 1174−1183.
(6) Chen, M.; Lan, X.; Tang, X.; Wang, Y.; Hudson, M. H.; Talapin, D. V.; Guyot-Sionnest, P. High carrier mobility in HgTe quantum dot solids improves Mid-IR Photodetectors. *ACS Photonics* **2019**, *6* (9), 2358−2365.
(7) Deng, Z.; Jeong, K. S.; Guyot-Sionnest, P. Colloidal quantum dots intra-band photodetectors. *ACS Nano* **2014**, *8* (11), 11707−11714.
(8) Klem, E. J. D.; Gregory, C.; Temple, D.; Lewis, J. PbS colloidal quantum dot photodiodes for low-cost SWIR sensing. *Proc. SPIE* **2015**, *9451*, 945104.
(9) Hafiz, S. B.; Al Mahfuz, M. M.; Ko, D.-K. Vertically stacked intra-band quantum dot devices for mid-wavelength infrared photodetection. *ACS Appl. Mater. Interfaces* **2021**, *13* (1), 937−943.
(10) Chen, M.; Shen, G.; Guyot-Sionnest, P. Size distribution effects on mobility and intra-band gap of HgSe quantum dots. *J. Phys. Chem. C* **2020**, *124* (29), 16216−16221.
(11) Ramiro, I.; Özdemir, O.; Christodoulou, S.; Gupta, S.; Dalmases, M.; Torre, I.; Konstantatos, G. Mid- and Long-wave infrared optoelectronics via intra-band transitions in PbS colloidal quantum dots. *Nano Lett.* **2020**, *20* (2), 1003−1008.
(12) Guyot-Sionnest, P.; Shim, M.; Matranga, C.; Hines, M. Intraband relaxation in CdSe quantum dots. *Phys. Rev. B* **1999**, *60* (4), 2181−2184.
(13) Wang, C.; Shim, M.; Guyot-Sionnest, P. Electrochromic nanocrystal quantum dots. *Science* **2001**, *291* (5512), 2390−2392.
(14) Norris, D. J.; Efros, A. L.; Erwin, S. C. Doped nanocrystals. *Science* **2008**, *319* (5871), 1776−1779.
(15) Sahu, A.; Kang, M. S.; Kompch, A.; Notthoff, C.; Wills, A. W.; Deng, D.; Winterer, M.; Frisbie, C. D.; Norris, D. J. Electronic impurity doping in CdSe nanocrystals. *Nano Lett.* **2012**, *12* (5), 2587−2594.
(16) Qu, J.; Goubet, N.; Livache, C.; Martinez, B.; Amelot, D.; Gréboval, C.; Chu, A.; Ramade, J.; Cruguel, H.; Ithurria, S.; et al. Intraband mid-infrared transitions in Ag_2Se nanocrystals: potential and limitations for Hg-Free low-cost photodetection. *J. Phys. Chem. C* **2018**, *122* (31), 18161−18167.
(17) Livache, C.; Martinez, B.; Goubet, N.; Gréboval, C.; Qu, J.; Chu, A.; Royer, S.; Ithurria, S.; Silly, M. G.; Dubertret, B.; Lhuillier, E. A colloidal quantum dot infrared photodetector and its use for intraband detection. *NAT. COMM.* **2019**, *10*, 2125.
(18) Hafiz, S. B.; Al Mahfuz, M. M.; Lee, S.; Ko, D.-K. Midwavelength infrared p−n heterojunction diodes based on intraband colloidal quantum dots. *ACS Appl. Mater. Interfaces* **2021**, *13* (41), 49043−49049.
(19) Yang, J.; Hu, H.; Lv, Y.; Yuan, M.; Wang, B.; He, Z.; Chen, S.; Wang, Y.; Hu, Z.; Yu, M.; et al. Ligand-Engineered HgTe colloidal quantum dot solids for infrared photodetectors. *Nano Lett.* **2022**, *22* (8), 3465−3472.
(20) Zhang, S.; Bi, C.; Tan, Y.; Luo, Y.; Liu, Y.; Cao, J.; Chen, M.; Hao, Q.; Tang, X. Direct optical lithography enabled multispectral colloidal quantum-dot imagers from ultraviolet to short-wave infrared. *ACS Nano* **2022**, *16* (11), 18822−18829.
(21) Beck, W. A. Photoconductive gain and generation recombination noise in multiple quantum-well infrared detector. *Appl. Phys. Lett.* **1993**, *63* (26), 3589−3591.
(22) Chen, M.; Guyot-Sionnest, P. Reversible electrochemistry of mercury chalcogenide colloidal quantum dot films. *ACS Nano* **2017**, *11* (4), 4165−4173.
(23) Goubet, N.; Jagtap, A.; Livache, C.; Martinez, B.; Portalès, H.; Xu, X.; Lobo, R. P. S. M.; Dubertret, B.; Lhuillier, E. Terahertz HgTe nanocrystals: beyond confinement. *J. Am. Chem. Soc.* **2018**, *140* (15), 5033−5036.
(24) Hao, Q.; Tang, X.; Cheng, Y.; Hu, Y. Development of flexible and curved infrared detectors with HgTe colloidal quantum dots. *Infrared Physics and Technology* **2020**, *108*, 103344.
(25) Zhang, C.; Xia, Y.; Zhang, Z.; Huang, Z.; Lian, L.; Miao, X.; Zhang, D.; Beard, M. C.; Zhang, J. Combination of cation exchange and quantized ostwald ripening for controlling size distribution of lead chalcogenide quantum dots. *Chem. Mater.* **2017**, *29* (8), 3615−3622.

https://doi.org/10.1021/acsomega.3c00403
ACS Omega 2023, 8, 19137−19144